Formation of ordered CoAl alloy clusters by the plasma-gas condensation technique

Toyohiko J. Konno[a] and Saeki Yamamuro[b]
Institute for Materials Research, Tohoku University, Sendai, 980-8577, Japan

Kenji Sumiyama
Department of Materials Science and Engineering, Nagoya Institute of Technology, Nagoya 466-8555, Japan

(Received 24 January 2001; accepted for publication 22 June 2001)

Co_xAl_{1-x} alloy clusters were synthesized from a mixture of Co and Al metal vapors generated by the sputtering of pure metal targets. We observed that the produced alloy clusters were uniform in size, ranging from approximately 20 nm for Al-rich clusters to 10 nm for Co-rich clusters. For a wide average composition range ($x \approx 0.4-0.7$), the alloy clusters have the ordered $B2$ (CsCl-type) structure. In the Co-rich cluster aggregates ($x=0.76$), the clusters are composed of face-centered-cubic (fcc) Co and minor CoAl($B2$) clusters. In the Al-rich aggregates ($x=0.23$), the clusters are mainly composed of the fcc-Al phase, although clusters occasionally possess a ''core-shell structure'' with the CoAl($B2$) phase surrounded by an Al-rich amorphous phase. These observations are in general agreement with our prediction based on the equilibrium phase diagram. We also noticed that the average composition depends not only on the relative amount of Co and Al vapors, but also on their absolute amount, and even on the Ar gas flow rate, which promotes mixing and cooling the two vapors. These findings show that the formation of alloy clusters in vapor phase is strongly influenced by the kinetics of cluster formation, and is a competing process between the approach to equilibrium and the quenching of the whole system. © *2001 American Institute of Physics.* [DOI: 10.1063/1.1394918]

I. INTRODUCTION

Nanostructurally tailored materials are expected to become the basis of the infrastructure of next-generation devices.[1] A number of studies have reported that granular solids and nanocrystalline materials exhibit fascinating magnetic,[2–4] transport,[5,6] optical,[7,8] and mechanical properties.[9,10] In these material designs, nanometer-sized granules or clusters serve as elemental functional units. Thus, a key to the success of this technology is the ability to control the structure and size of the clusters. We have recently developed a plasma-gas condensation (PGC) type cluster deposition apparatus, in which clusters, several nanometers to several ten of nanometers in diameter, can be formed directly from the metal vapors produced by the sputtering of a target material.[11] Since this is a sputter-based vapor-phase synthesis of clusters, a wide variety of elements can serve as source materials.[12] Recently, it has been demonstrated that the PGC technique allows the production of monodispersively sized metal clusters such as Cr, Co, and Ni.[13–15]

Although from an application point of view, the stable formation of alloy clusters is highly desired, the formation of intermetallic alloy clusters by this method has not been proved. The fact that sputtering can generate almost any kind of metal vapors makes the PGC technique particularly attractive. However, the synthesis of alloy clusters involves a number of difficulties that are not encountered in the formation of elemental metal clusters. For example, two kinds of metal vapors must collide with each other in the vapor phase, react to form the alloy, cool sufficiently, and grow in the vapor to become clusters desirably uniform in size. This process depends heavily on a number of processing parameters, such as relative and absolute amounts of metal vapors, kinds of carrier gas, metal vapor mixing methods, and vapor cooling by the carrier gas, among others.

The formation of metal clusters by vapor-phase synthesis may be qualitatively understood by the traditional nucleation and growth model.[16] However, the validity of the assumption of dynamical equilibrium between the solid phase (cluster) and the vapor(s) is not obvious. In other words, cluster formation is likely to be dictated by the number of parameters that are irreversible in nature. These include rapid quenching of the metal vapors by the Ar carrier gas and its flow rate, which must compete with the approach to the equilibrium.

In this regard, achieving the synthesis of alloy clusters that possess an ordered structure represents quite a challenge. This article describes our attempt to produce uniformly sized intermetallic alloy clusters in the vapor phase. We chose the Co–Al system because of the well-known stability of the ordered $B2$ (CsCl-type) structure.[17,18] Our results show that the production of uniformly sized CoAl($B2$) alloy clusters depends not only on the relative amounts of source materials, but also on their absolute amounts, and other processing conditions such as flow rate of the carrier gas.

[a]Electronic mail: tjkonno@imr.tohoku.ac.jp
[b]Present address: Department of Physics, Carnegie-Mellon University, Pittsburgh, PA 15213.

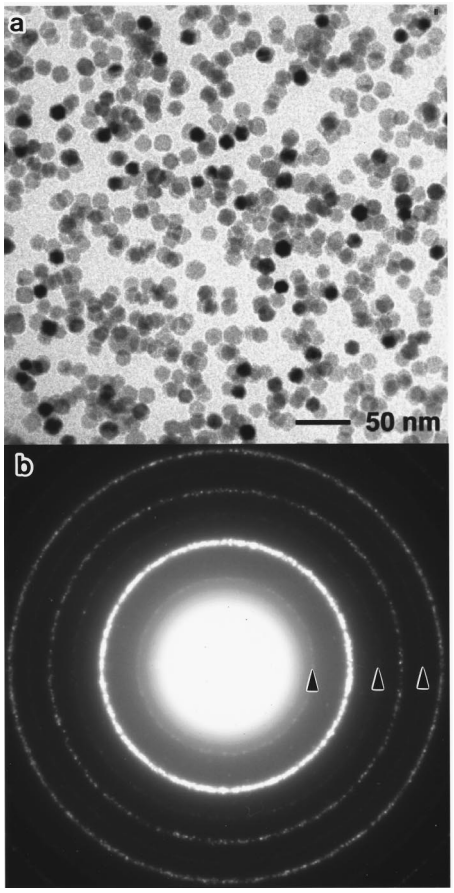

FIG. 1. (a) Bright-field TEM image of CoAl alloy clusters with an average composition of 54 at. % Co. Ar gas flow rate: 300 sccm; sputtering power: 250 W for both Co and Al targets. (b) Corresponding electron diffraction pattern. The arrowed rings are {100}, {111}, and {210}, and suggest the formation of the $B2$(CsCl-type) structure.

II. EXPERIMENTAL PROCEDURES

We used a magnetron sputtering system with Co and Al targets 80 mm in diameter, controlled independently for the generation of metal vapors. The two targets were placed face to face, separated by 100 mm.[13] The input power of each target was controlled in the range of 100–300 W. A large amount of Ar gas of 200–400 standard cubic centimeters per minute (sccm) was introduced continuously into the sputtering chamber, making the pressure inside the chamber approximately 130 Pa. This unusually high Ar pressure restricts the glow discharge region to only several mm above each target, allowing us to control the power of the targets independently despite the fact that the targets are placed face to face for the different elements to mix effectively. The metal vapors thus generated were swept into the growth region (approximately 10 cm in length, set at the liquid-nitrogen temperature), together with an Ar carrier gas through an aperture 3.5 mm in diameter by a mechanical booster pump. There was also an aperture of the same size at the exit of the growth region. The clusters coming out of the aperture were led to the deposition chamber (less than about 1×10^{-2} Pa) through two skimmers by differential pumping. The clusters were finally deposited on carbon-coated colodion films supported by Cu grids at room temperature for transmission

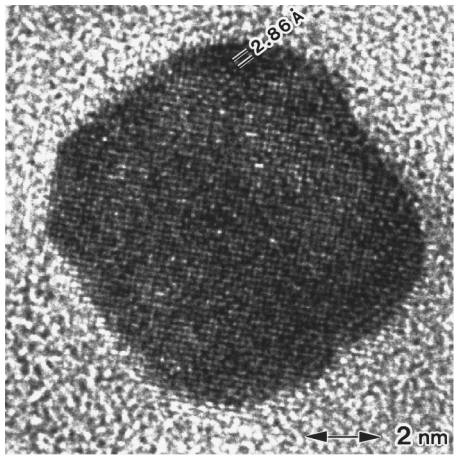

FIG. 2. High-resolution TEM image of a CoAl cluster in the cluster aggregate shown in Fig. 1. Note that this cluster has prominent {100} facets together with minor {110} facets.

electron microscopy (TEM) observations. We used a Hitachi HF-2000 transmission electron microscope operating at 200 kV for structural characterization. This microscope was equipped with x-ray energy-dispersive spectroscopy (EDS), which was used for compositional analyses. The zero-field-cooled (ZFC) and field-cooled (FC) thermomagnetic curves at magnetic field H of 100 Oe was measured for cluster aggregates of 54 at. % Co by a superconducting quantum interference device magnetometer.

III. EXPERIMENTAL RESULTS

Figure 1(a) shows a bright-field (BF) TEM micrograph of the clusters produced at the sputtering power of 250 W for Co and Al targets, and at an Ar gas flow rate of 300 sccm. Figure 1(a) shows that the clusters are uniformly sized with an average diameter of approximately 14 nm. The average composition of the cluster aggregates determined by EDS was 54 at. % Co. Figure 1(b) is a corresponding electron diffraction (ED) pattern. The diffraction rings indicated by the arrows can be indexed as {100}, {111}, and {210} of the simple cubic structure, and show that the clusters possess the $B2$ (CsCl) structure. The lattice constant obtained from the ED pattern was 2.85 ± 0.02 Å, in agreement with the lattice constant of CoAl($B2$), 2.86 Å.

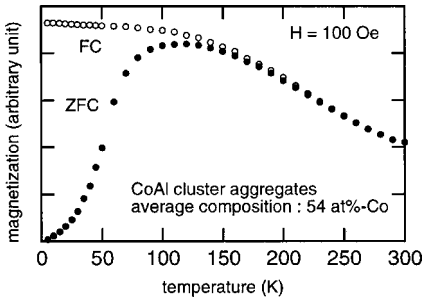

FIG. 3. Temperature dependence of the magnetization for the CoAl($B2$) cluster aggregates in the magnetic field of 100 Oe. The open circles indicate the field-cooled (FC) magnetization and the closed circles the zero-field-cooled (ZFC) magnetization.

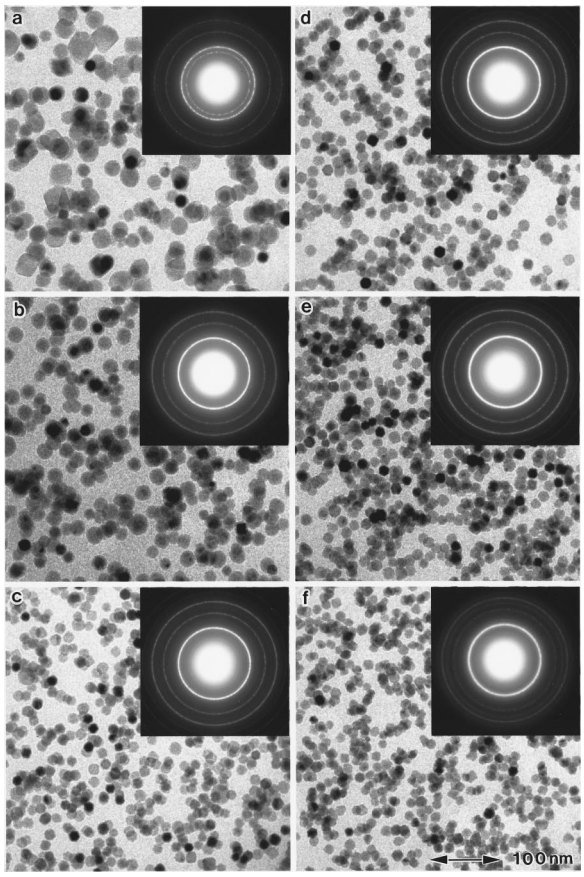

FIG. 4. Bright-field TEM images of CoAl alloy clusters, and electron diffraction patterns (insets). Ar gas flow rate: 300 sccm; sputtering power: Al target 100 W (fixed), and Co target: (a) 100 W; (b) 150 W; (c) 170 W; (d) 200 W; (e) 250 W; and (f) 300 W.

Figure 2 is a high-resolution TEM (HRTEM) micrograph of a cluster found in the same specimen. As shown here, the cluster is composed of a single grain and has a fourfold rotational symmetry. The major and minor facets are of the {100} and {110} planes, respectively, and the cluster is likely to possess a three-dimensionally faceted shape.

The Co–Al phase diagram shows that the CoAl($B2$) phase has a wide nonstoichiometric range in the Co-rich side of the stoichiometric composition of 1:1.[18] It is known that in the Co-rich CoAl($B2$) phase, the excess Co atoms occupy Al sites, and bring in ferromagnetic coupling between the nearest Co–Co atoms.[19] Macroscopically, this magnetic ordering appears as paramagnetic[20–22] and spin-glass[23] behaviors in thermomagnetization curves.

Figure 3 shows the FC and ZFC curves obtained for CoAl($B2$) cluster aggregates with an average composition of 54 at. % Co. The magnetization is in the arbitrary unit since we were not able to measure the total weight of the clusters. Nevertheless, the ZFC magnetization curve clearly shows that this cluster assembly possesses the blocking temperature of approximately 170 K, as defined by the onset of irreversibility. This is in good agreement with the reported behavior of the susceptibility of Co-rich CoAl($B2$) bulk materials,[23] showing that the ferromagnetic coupling due to Co–Co neighboring does exist in the vapor-synthesized CoAl($B2$) clusters. This observation indicates that the nearest neighbors of Co atoms in the clusters do not differ significantly from those in the bulk material, and suggests Co and Al atoms were mixed reasonably well during the cluster formation.

Figure 4 is a series of BF-TEM micrographs of the cluster aggregates prepared when the power of Al was fixed to 100 W, while that of Co was varied from (a) 100 W, (b) 150 W, (c) 170 W, (d) 200 W, (e) 250 W, to (f) 300 W. The Ar gas

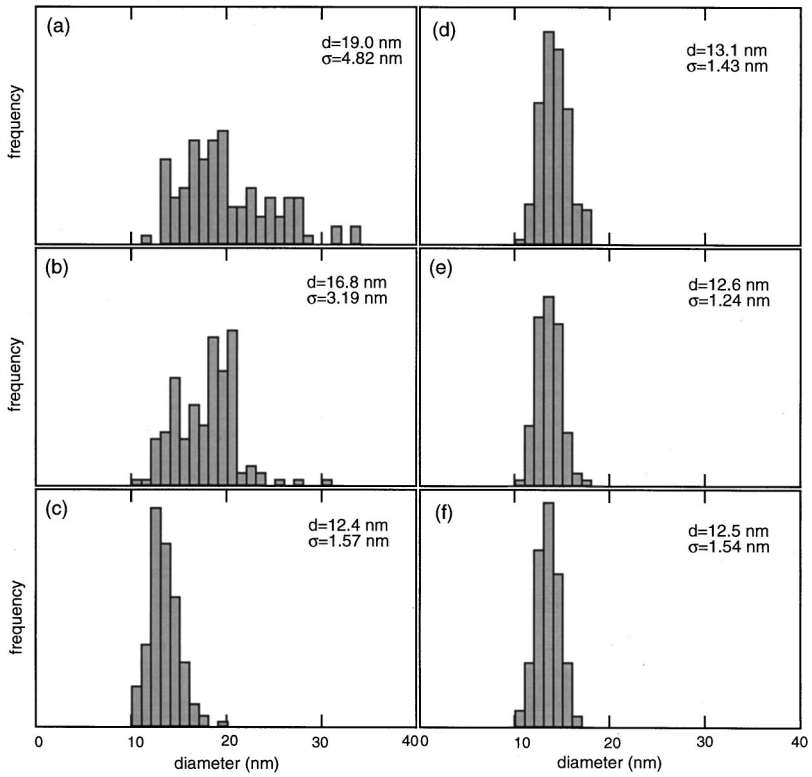

FIG. 5. Size distribution of the CoAl alloy clusters shown in Fig. 4. Also indicated in the figures are the average diameter and standard deviation.

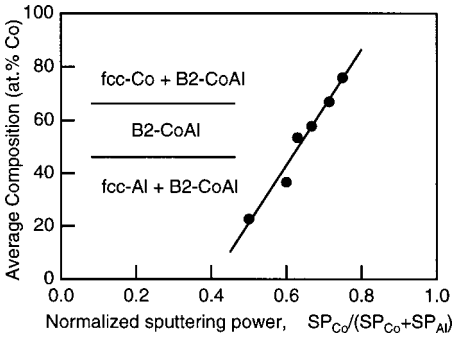

FIG. 6. Composition of the CoAl alloy clusters shown in Fig. 4 as a function of the normalized sputtering power ratio. Composition was obtained by EDS analysis, while the structure was determined from the diffraction patterns.

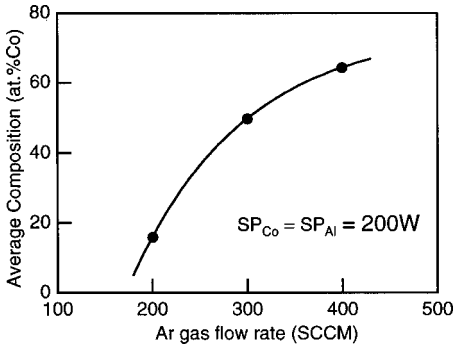

FIG. 8. Effect of the Ar gas flow rate on the average composition of CoAl cluster aggregates, showing that the mixing of the metal vapors by the Ar carrier gas is a prerequisite for the CoAl alloy formation.

flow rate was 300 sccm for all cases. The inset ED pattern (a) can be ascribed to the fcc-Al phase, (b)–(e) to the CoAl($B2$) phase, and (f) to the mixture of the fcc-Co phase and minor CoAl($B2$) phase.

Figure 5 shows the size distribution, average diameter, and standard deviation of the clusters shown in Fig. 4. As shown here, the cluster size becomes monodispersive with increasing the power of Co, with the average cluster size of approximately 12–13 nm.

The average composition of the same cluster aggregates, as determined from the EDS analysis, was 23, 37, 54, 58, 67, and 76 at. % Co, respectively. These values were plotted as a function of the normalized ratio of the sputtering power of the two targets in Fig. 6, which shows that the average composition is a linear function of the ratio of the sputtering power of the two targets.

Figure 7 shows the average composition of the cluster aggregates obtained when the sputtering powers of both the Co and Al targets were changed from 100 to 300 W and the ratio was fixed to 1:1. As shown here, the average composition of the cluster aggregates changes even when the ratio of the sputtering power remains constant, and it saturates to approximately 50 at. % Co as the power of both targets increases.

Figure 8 shows the effect of the Ar gas flow rate on the average composition of the cluster aggregates. The power of Co and Al targets was fixed to 200 W, but the flow rate was increased from 200 to 400 sccm. As Fig. 8 shows, the average composition was below 20 at. % Co when the Ar gas flow rate was 200 sccm, but when the flow rate was increased to 300 sccm, it was close to 50 at. % Co. Thus, the average composition of the clusters depends not only on the relative amount of the power, but also on the absolute amount of the power and Ar gas flow rate.

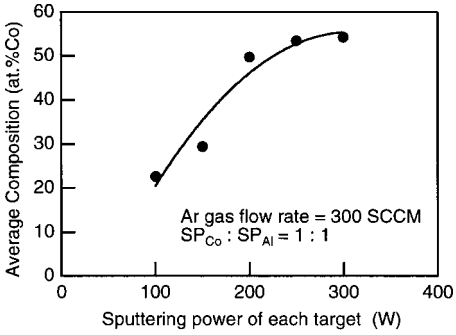

FIG. 7. Effect of total sputtering power on an average composition of CoAl cluster aggregates. This figure indicates that the composition of clusters becomes 1:1 when metal vapors of Co and Al are sufficiently supplied in the chamber.

Figure 9(a) shows a BF-TEM micrograph of a cluster aggregate with the average composition of 18 at. % Co. In this Al-rich cluster aggregate, we often found, among the uniformly contrasted clusters, a cluster with a strong contrast in its ''core,'' but a uniform gray contrast in its ''shell.'' Arrow A in Fig. 9(a) indicates one such cluster, while arrow B points to a uniformly contrasted cluster. Figure 9(b) is a HRTEM micrograph of the core–shell cluster observed in the same aggregate. The lattice fringe 2.86 Å found in the core suggests that it is composed of the $B2$ structure. It should be noted that we failed to detect any distinct lattice fringes from the shell of the same cluster. In fact, the image contrast in the shell suggests that the shell is composed of an amorphous phase. Figure 9(c) is a set of EDS profiles taken from clusters A and B indicated in Fig. 9(a). These profiles show that the ''average'' composition of core–shell cluster A is 52 at. % Co while that of B is 19 at. %. These results, especially the fact that the core–shell cluster is rich in Co, support the view that the core of cluster A is made up of the $B2$ phase.

IV. DISCUSSION

We showed that monodispersive single-phase CoAl alloy clusters with the $B2$ structure can be formed by vapor-phase synthesis. The $B2$ phase was found to dominate in cluster aggregates of approximately 40–70 at. % Co. We also showed that the average composition of cluster aggregates depends heavily on processing conditions; in fact, it is a function of not only the ratio of the sputtering powers of Co and Al targets, but also of other processing parameters, such as total sputtering power and Ar gas flow rate.

The CoAl($B2$) alloy clusters were uniform in size, and grew to about 12–14 nm, often exhibiting a faceted shape. This implies that an alloy cluster can grow into the equilibrium shape[24] provided there is a sufficient supply of constituents from the vapor. Moreover, the spin-glass behavior ob-

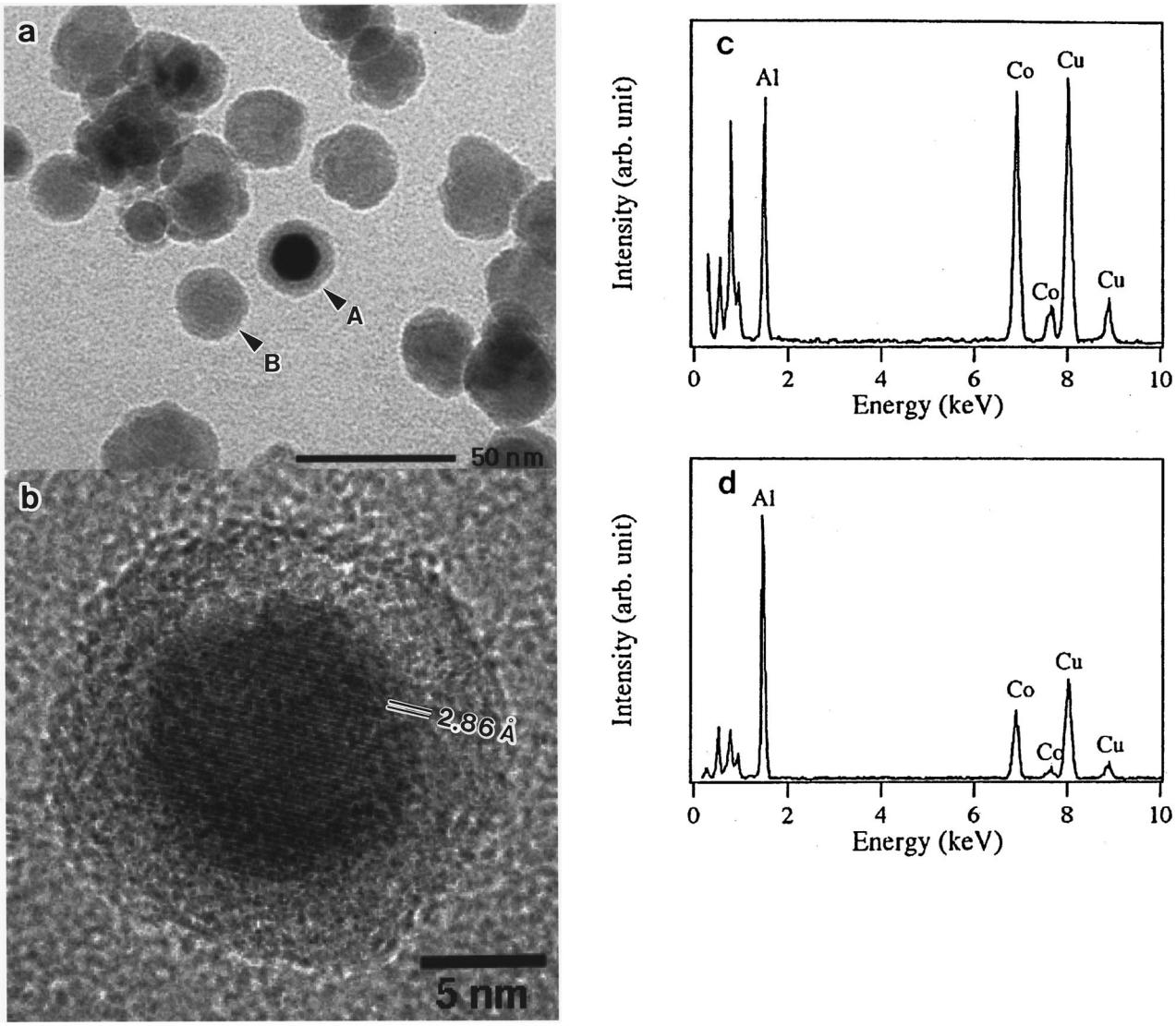

FIG. 9. (a) Bright-field TEM micrograph of CoAl alloy clusters of an average composition of 18 at. % Co. The cluster indicated by arrow A has a core–shell structure, while the one indicated by arrow B shows a uniform gray contrast. Note that the core of the cluster has a faceted shape. (b) High-resolution TEM micrograph of a cluster, found in the same cluster aggregates. The lattice fringe 2.86 Å suggests that the core is composed of the CoAl($B2$) phase, while the shell exhibits an amorphous structure. (c) and (d) EDS profiles of the clusters indicated by arrows A and B, respectively, in (a).

served in 54 at. % Co cluster aggregates indicates the ferromagnetic interaction of Co atoms inside the CoAl($B2$) clusters, and shows that the clusters possess a defect structure similar to the Co-rich bulk CoAl($B2$) materials. On the other hand, the Co–Al phase diagram shows that Co atoms can dissolve in the $B2$ phase only up to about 56 at. % Co at 300 °C, while at 1200–1450 °C the ordered $B2$ phase can exist in a wide composition range, i.e., about 46 at. % Co to more than 70 at. % Co.[18] Therefore, the relatively wide composition range for the CoAl($B2$) clusters observed in the present investigation indicates that cluster formation took place at a relatively high temperature, and that the clusters are ''quenched'' into room temperature by collision with Ar carrier gas. These apparently contradicting observations suggest that the formation of alloy clusters is a competing process between the approach to equilibrium and the quenching of the whole system.

Yamamuro, Sumiyama, and Suzuki have demonstrated, based on their vapor-phase synthesis of elemental Cr clusters, that the prerequisites for uniformity of cluster size are the limited nucleation period and growth afterwards, the two being clearly separated.[13] The uniformity of the CoAl($B2$) clusters shown in Fig. 1 suggests that the two kinds of metal vapors were sufficiently present and mixed so that they were supersaturated against the formation of the CoAl($B2$) phase. Since the size of the clusters was uniform, and the structure inside the cluster was also homogeneous, we may infer that the CoAl($B2$) phase nucleated homogeneously in the Ar-cooled vapor phase.

We also observed that the absolute applied power of the Co and Al targets, together with the Ar gas flow rate, are important processing factors for the stable production of CoAl($B2$) clusters. The sputtering yields of Co and Al are reported to be within 15% of each other, and they are essen-

tially proportional to the applied power.[25] We can, therefore, suggest that the effect of the absolute sputtering power is to increase the number density of the two kinds of metal vapors, thereby increasing the chance for them to collide and react. Once supersaturated, the large driving force for the formation of the CoAl($B2$) phase (e.g., the heat of formation $\Delta H°$ is about -110 kJ/mol CoAl from the solid Co and Al phases) favors the formation of this phase over the formation of the elemental Al and Co phases.[26] The latter phases may nucleate, but a large number of collisions (approximately 1.5×10^5 Co and Al atoms are required to form a 15 nm diam cluster) averages out the possibility of the growth of the elemental phases.

It was shown previously that for the formation of elemental Cr clusters, an increase in Ar gas flow rate of up to 1200 sccm resulted in the broadening of the cluster size distribution.[13] This is because the nucleation process is ''carried away'' to the growth region, thereby giving a chance for the clusters to nucleate continuously. In the present investigation, the decrease in Ar gas flow rate from 400 to 200 sccm resulted in the unexpected disappearance of CoAl clusters and the appearance of Al-rich clusters. This shows that a certain flow rate of the carrier gas is necessary to mix the two kinds of metal vapors for the formation of alloy clusters.

When Co and Al vapors are not sufficiently mixed, we initially assumed that the Co and Al clusters would form separately when the ratio of the sputtering power was close to 1:1. However, we noticed that the average composition of the cluster aggregates became Al-rich under these conditions despite the fact that the chamber was constructed in a perfectly symmetric configuration with respect to the Co and Al source. This suggests that nucleation and growth are much easier for Al clusters than for Co clusters, but we are still unable to justify this large asymmetry in cluster forming ability. A simple calculation of the free-energy change upon solidification suggests that the driving force will be large for Co cluster formation. For example, the heat of formation $\Delta H°$ of Al and Co from the gaseous phase is about -330 and -430 kJ/mol for Al and Co, respectively (standard state taken at 298 K),[26] while the classical collision model suggests that the cooling efficiency for Co vapor by Ar gas is only slightly smaller than for Al because of the small atomic mass difference, i.e., 27, 40, and 59, for Al, Ar, and Co, respectively. These rather simplistic thermodynamical considerations suggest that the driving force for Co cluster formation should be larger than that for Al clusters, contrary to the experimental results described here. Thus, the asymmetry is probably due to certain kinetic factors governing the vapor-phase synthesis of the cluster formation.

The Co-rich cluster aggregates consist of fcc-Co clusters about 10 nm in diameter. Although hexagonal closed-packed (hcp) Co is stable in bulk at room temperature,[27] fine particles often exhibit fcc Co.[28,29] Our previous observation on pure Co clusters prepared using the same apparatus also showed that fcc Co is the major constituent when the diameter is less than 10 nm.[14] In addition, the phase diagram indicates that the solubility of Al in hcp Co at temperatures below 400 °C is negligible, but up to 15 at. % of Al can be dissolved in fcc Co at 1400 °C.[18] Thus, if our clusters retain their structure at a high temperature, as suggested by the wide composition range of the obtained CoAl($B2$) clusters, we may consider that the fcc-Co phase stabilized by the Al dissolution was quenched at room temperature.

In the Al-rich region, the diffraction pattern of the cluster aggregates showed that clusters are composed of the fcc-Al phase; whereas close examination of individual clusters revealed that some of the clusters are composed of a core having the CoAl($B2$) phase and a shell that shows a contrast typical to an amorphous structure. Core–shell structures that have been found in the past are composed of metal core and oxide shell.[30,31] We can suggest that the core–shell structure was most likely brought about by a shortage of Co vapors: the CoAl($B2$) phase was nucleated sporadically, but it could not grow continuously. The Al–Co phase diagram shows that there are four intermetallic compounds with low solubility in the composition range of 18–28 at. % Co.[18] Thus, we may infer that the formation of these complex compounds was suppressed due to rapid quenching in the vapor phase, and resulted in an Al-rich amorphous alloy, which heterogeneously nucleated on the CoAl($B2$) core and grew.

To summarize, the present investigation showed that the formation of alloy clusters is a strong function of the extent of the supersaturation and supercooling of metal vapors, which varies locally inside the chamber and depends heavily on processing conditions. Thus, in order to produce alloy clusters of uniform size and composition, a sufficient amount of metal vapors must be supplied and mixed effectively. This will result in the homogeneous nucleation and subsequent growth of the CoAl($B2$) clusters.

V. SUMMARY

We employed a plasma-gas aggregation technique to produce intermetallic CoAl alloy clusters. It was observed experimentally that cluster formation is not only a function of the ratio of the vapors supplied, but also of their total amount and the manner in which they mix and react. When both Co and Al vapors were sufficiently supplied and mixed, uniformly sized CoAl clusters with the $B2$ structure were obtained in the composition range of 37–67 at. % Co, a range considerably wider than that expected from the equilibrium phase diagram. In the Co-rich side, the fcc-Co phase containing Al was formed. In the Al-rich side, the fcc-Al phase was the dominant constituent, with clusters having a CoAl($B2$) core surrounded by an amorphous phase being frequently observed. These observations suggest that cluster formation in the vapor phase is a competing process between the approach to the equilibrium and the quenching of the whole system.

ACKNOWLEDGMENT

This work was supported by Core Research for Evolutional Science and Technology (CREST) of the Japan Science and Technology Corporation (JST).

[1] R. P. Andres, R. S. Averback, W. L. Brown, L. E. Brus, W. A. Goddard III, A. Kaldor, S. G. Louie, M. Moscovits, P. S. Peercy, S. J. Riley, R. W. Siegel, F. Spaepen, and Y. Wang, J. Mater. Res. **4**, 704 (1989).
[2] C. L. Chien, J. Appl. Phys. **69**, 5267 (1991).

[3] J. P. Chen, C. M. Sorensen, K. J. Klabunde, and G. C. Hadjipanayis, Phys. Rev. B **51**, 11527 (1995).
[4] B. Barbara, J. Magn. Magn. Mater. **156**, 123 (1996).
[5] P. Sheng, B. Abeles, and Y. Arie, Phys. Rev. Lett. **31**, 44 (1973).
[6] A. E. Berkowitz, J. R. Mitchell, M. J. Carey, A. P. Young, S. Zhang, F. E. Spada, F. T. Parker, A. Hutten, and G. Thomas, Phys. Rev. Lett. **68**, 3745 (1992).
[7] J. P. Wilcoxon, R. L. Williamson, and R. Baughman, J. Chem. Phys. **98**, 9933 (1993).
[8] A. P. Alvisatos, MRS Bull. **20**, 23 (1995).
[9] B. M. Clemens, H. Kung, and S. A. Barnett, MRS Bull. **24**, 20 (1999).
[10] J. R. Weertman, D. Farkas, K. Hemker, H. Kung, M. Mayo, R. Mitra, and H. Van Swygenhoven, MRS Bull. **24**, 44 (1999).
[11] S. Yamamuro, M. Sakurai, K. Sumiyama, and K. Suzuki, AIP Conf. Proc. **416**, 491 (1998).
[12] H. Haberland, M. Karrais, M. Mall, and Y. Thurner, J. Vac. Sci. Technol. A **10**, 3266 (1992).
[13] S. Yamamuro, K. Sumiyama, and K. Suzuki, J. Appl. Phys. **85**, 483 (1999).
[14] S. Yamamuro, K. Sumiyama, T. J. Konno, and K. Suzuki, Mater. Trans., JIM **40**, 1450 (1999).
[15] T. Hihara and K. Sumiyama, J. Appl. Phys. **84**, 5270 (1998).
[16] J. W. Christian, *The Theory of Transformations in Metals and Alloys*, 2nd ed. (Pergamon, Oxford, 1990).
[17] C. Müller, H. Wonn, W. Blau, P. Zieshe, and V. P. Krivitskii, Phys. Status Solidi B **95**, 215 (1979).
[18] A. J. McAlister, in *Binary Alloy Phase Diagrams*, 2nd ed., edited by T. B. Massalski (ASM International, Materials Park, OH, 1990), pp. 136–138.
[19] E. Wachtel, V. Linse, and V. Gerold, J. Phys. Chem. Solids **34**, 1461 (1973).
[20] G. W. West, Philos. Mag. **15**, 855 (1967).
[21] K. Miyatani and S. Iida, J. Phys. Soc. Jpn. **25**, 1008 (1968).
[22] A. N. Bashikatov, L. P. Zelenin, F. A. Sidorenko, and P. V. Gel'd, Phys. Met. Metallogr. **31**, 46 (1971).
[23] E. Lähderanta, K. Eftimova, R. Laiho, H. Al Kanani, and J. G. Booth, J. Magn. Magn. Mater. **130**, 23 (1994).
[24] L. D. Marks, Rep. Prog. Phys. **57**, 603 (1994).
[25] J. L. Vossen and W. Kern, *Thin Film Processes* (Academic, New York, 1978), p. 15.
[26] O. Kubashewski and C. B. Alcock, *Metallurgical Thermochemistry* (Pergamon, Oxford, 1979).
[27] J. T. Plewes and K. J. Bachmann, Metall. Trans. **4**, 1729 (1973).
[28] H. Sato, O. Kitakami, T. Sakurai, Y. Shimada, Y. Otani, and K. Fukamichi, J. Appl. Phys. **81**, 1858 (1997).
[29] O. Kitakami, H. Sato, Y. Shimada, F. Sato, and M. Tanaka, Phys. Rev. B **56**, 13849 (1997).
[30] S. Gangopadhyay, G. C. Hadjipanayis, C. M. Sorensen, and K. J. Klabunde, IEEE Trans. Magn. **29**, 2602 (1993).
[31] D. L. Peng, K. Sumiyama, T. J. Konno, T. Hihara, and S. Yamamuro, Phys. Rev. B **60**, 2093 (1999).